

Impact excitation by hot carriers in carbon nanotubes

Vasili Perebeinos* and Phaedon Avouris†

T. J. Watson Research Center, IBM Research Division, Yorktown Heights, New York 10598, USA

(Received 17 July 2006; published 27 September 2006)

We investigate theoretically the efficiency of intramolecular hot-carrier-induced impact ionization and excitation processes in carbon nanotubes. The electron confinement and reduced screening lead to drastically enhanced excitation efficiencies over those in bulk materials. Strong excitonic coupling favors neutral excitations over ionization, while the impact mechanism populates a different set of states than that produced by photoexcitation. The excitation rate is strongly affected by optical phonon excitation and a simple scaling of the rate with the field strength and optical phonon temperature is obtained.

DOI: 10.1103/PhysRevB.74.121410

PACS number(s): 78.67.Ch, 72.20.Jv, 73.63.Fg, 78.60.Fi

The excellent electrical properties and direct gap of carbon nanotubes (CNTs) offer the possibility of a unified electronic and optoelectronic technology based on this material.¹ Electroluminescence (EL) in CNT field effect transistors has already been demonstrated, where electrons and holes were independently injected in an ambipolar device.^{2–4} Recently, light emission has been observed under unipolar transport conditions in the suspended tubes⁵ and from the CNT-metal contacts.^{4,6} In the suspended sample the light intensity is stronger by a factor of ~ 1000 compared to ambipolar devices. The mechanism of this enhanced EL was proposed to involve an unusually efficient intranotube impact excitation process involving the hot carriers in CNTs, generated by the high local fields at the interface between the suspended and nonsuspended parts of the tube and the metal-nanotube contact. By utilizing this impact excitation process in quasi-one-dimensional confined structures, high exciton densities can be achieved for probing the interactions of such boson systems and for generating ultra bright nanoscale light sources used in nanophotonics.

Here, we provide a detailed theoretical study of the impact excitation in semiconducting CNTs. In low-dimensional materials, the Coulomb interactions are weakly screened, and large exciton binding energies in CNTs have been predicted theoretically^{7–9} and verified experimentally.^{10–12} This presents an additional challenge for the computation of impact excitation rates in CNTs. We find that the impact scattering rate is very fast, up to five orders of magnitude larger than those in bulk semiconductors.¹³ This can be easily rationalized since the same Coulomb interactions responsible for the large exciton binding are also responsible for the impact excitation scattering. The electron-hole correlations in the final state make the impact excitation process, on the average, twice more efficient than the impact ionization, where the created electron-hole pairs are treated as independent particles. Impact excitation, generates a different initial distribution of excited states than that produced by photon excitation, due to the different selection rules and momentum conservation requirements.

It has recently been shown that under high bias the energetic carriers in nanotubes excite optical and zone-boundary phonons^{14–17} and generate a nonequilibrium phonon distribution,^{18,19} particularly when energy dissipation to the substrate is suppressed as in suspended CNTs.¹⁹ We have calculated the effect of optical phonon excitation and found

that the exciton production rate depends exponentially both on the hot phonon temperature and on the electric field, and the effect can be described by a simple scaling relation. As a result, optical phonon excitation significantly increases the EL intensity under unipolar transport conditions. The energy spectra of the excitons generated consist of several peaks corresponding to excitons with different angular momenta L : E_{11}^2 , E_{12}^3 , and E_{22}^4 , where E_{ij}^L stands for an exciton with electron and hole primarily from bands i and j . The relative intensities and the overall excitation efficiencies are functions of the electric field, the optical phonon temperature, and the CNT chirality.

The impact ionization scattering rate of an electron with momentum and energy $(k_1, \varepsilon_{k_1}^c)$ scattered to state $(k_1 - q, \varepsilon_{k_1 - q}^c)$ plus an e - h pair with a hole $(-k_2, -\varepsilon_{k_2}^v)$ and an electron $(k_2 + q, \varepsilon_{k_2 + q}^c)$ is given by²⁰

$$W_{k_1, k_1 - q} = \frac{2\pi}{\hbar} \sum_{k_2} |M_\nu|^2 \delta(\varepsilon_{k_1}^c - \varepsilon_{k_2}^v - \varepsilon_{k_1 - q}^c - \varepsilon_{k_2 + q}^c),$$

$$|M_\nu|^2 = |M_\nu^d - M_\nu^e|^2 + |M_\nu^d|^2 + |M_\nu^e|^2, \quad (1)$$

where $\nu = k_1 k_2 q$, and $M_\nu^d = J(k_1 k_2, k_2 + q k_1 - q)$ and $M_\nu^e = J(k_1 k_2, k_1 - q k_2 + q)$ are the direct and the exchange integrals:

$$J(k_1 k_2, k_1 - q k_2 + q) = \int d\vec{r}_1 d\vec{r}_2 \Psi_{ck_1}^*(\vec{r}_1) \Psi_{vk_2}^*(\vec{r}_2),$$

$$\Psi_{ck_1 - q}(\vec{r}_1) \Psi_{ck_2 + q}(\vec{r}_2) V(\vec{r}_1, \vec{r}_2). \quad (2)$$

$V(\vec{r}_1, \vec{r}_2)$ is the Coulomb potential screened by the dielectric environment of the nanotube⁹ and $\Psi_c(\vec{r})$ and $\Psi_v^*(\vec{r})$ are the electron and hole wave functions, given by a π -orbital tight-binding model with hopping matrix element $t = 3.0$ eV. In Eq. (1) we neglect e - h pair occupation in the initial state and, hence, processes where the electron can absorb an e - h pair.

To include the effect of e - h correlation in the final state we follow Ref. 21 and show that the impact excitation scattering rates due to the production of singlet (S) and triplet (T) excitons are given by

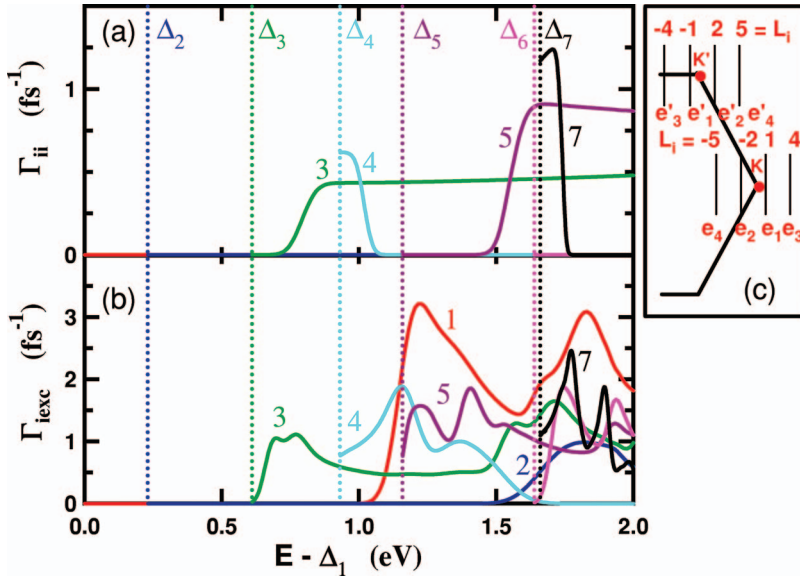


FIG. 1. (Color) (a) Impact ionization rates and (b) impact excitation rates for a (25,0) nanotube ($d=2.0$ nm) as a function of energy (measured from the bottom of the first conduction band Δ_1), for the first seven conduction bands shown in red, blue, green, cyan, magenta, light red, and black in increasing order of the band index. The vertical dashed lines correspond to the bottoms of the conduction bands Δ_i ($i=2,3,\dots,7$) relative to Δ_1 . (c) The vertical lines are allowed k points of zigzag tube with $\text{mod}(n,3)=1$ for the first four doubly degenerate bands $e_i^{L_i}$ ($e_i'^{L_i}$). The angular momenta L_i , in units of $2/(3d)$, measures a minimum distance from the K (K') point of graphene to the 1D lines of allowed k points of a nanotube. Note that the hole momentum has the opposite sign to that of the electron momentum.

$$\begin{aligned}
 W_{k_1 k_1 - q}^S &= \frac{\pi}{\hbar} \sum_{\mu} |\tilde{M}_{k_1 q \mu}^S|^2 \delta(\varepsilon_{k_1}^c - \varepsilon_{k_1 - q}^c - E_{q\mu}^S), \\
 W_{k_1 k_1 - q}^T &= \frac{\pi}{\hbar} \sum_{\mu} |\tilde{M}_{k_1 q \mu}^T|^2 \delta(\varepsilon_{k_1}^c - \varepsilon_{k_1 - q}^c - E_{q\mu}^T), \\
 |\tilde{M}_{k_1 q \mu}^S|^2 &= |\tilde{M}_{k_1 q \mu}^d - \tilde{M}_{k_1 q \mu}^e|^2 + |\tilde{M}_{k_1 q \mu}^d|^2, \\
 |\tilde{M}_{k_1 q \mu}^T|^2 &= |\tilde{M}_{k_1 q \mu}^d - \tilde{M}_{k_1 q \mu}^e|^2 + |\tilde{M}_{k_1 q \mu}^d|^2 + 2|\tilde{M}_{k_1 q \mu}^e|^2, \\
 \tilde{M}_{k_1 q \mu}^d &= \sum_{k_2} A_{k_2 q}^{\mu} M_{k_1 k_2 q}^d, \\
 \tilde{M}_{k_1 q \mu}^e &= \sum_{k_2} A_{k_2 q}^{\mu} M_{k_1 k_2 q}^e,
 \end{aligned} \quad (3)$$

where $E_{q\mu}^S$ and $E_{q\mu}^T$ are the singlet and triplet exciton transition energies,²² A_{kq}^{μ} is the solution of the Bethe-Salpeter equation^{8,9} for the exciton two-particle wavefunction

$$\Phi_q^{\mu}(\vec{r}_1, \vec{r}_2) = \sum_k A_{kq}^{\mu} \Psi_{ck+q}^{\mu}(\vec{r}_1) \Psi_{vk}^{\mu*}(\vec{r}_2). \quad (4)$$

We model the screening of the Coulomb interaction by the dielectric constant of the medium embedding the nanotube,⁹ for both the Bethe-Salpeter equation kernel and the impact ionization Coulomb potential Eq. (2). The CNT diameter dependence of exciton binding energies obtained by two-photon fluorescence excitation spectroscopy²³ agrees very well with our model calculations⁹ by choosing $\epsilon=3.3$, a value that we use in the rest of the paper.

The impact ionization and impact excitation scattering rates for a tube of diameter $d=2$ nm are shown in Figs. 1(a) and 1(b), respectively. This is a typical diameter of tubes used in opto-electronic applications and grown by chemical vapor deposition. The impact excitation rates in CNTs are roughly twice as large as the impact ionization rates due to the e - h confinement in the final state. To understand the structure of the impact ionization scattering rates in Fig. 1(a), we need to consider the implications of energy and momentum conservation. The momentum has two components: a

discrete angular momentum, which labels the bands, and a linear momentum along the tube axis. The CNT bands are nonparabolic and the angular momentum conservation law plays a crucial role in determining the threshold energy of the impact excitation.²⁴ As seen from Fig. 1(c), angular momentum conservation allows electrons in the third, e_3 , and the fourth, e_4 , bands to undergo impact ionization scattering by creating electron-hole pairs in the first and the second bands, respectively: $e_3^4 = e_2'^2 + e_1^1 + h_1'^1$ and $e_4^5 = e_1^1 + e_2'^2 + h_2^2$, where the superscript is the angular momentum in units of $2/(3d)$. The prime indicates that the corresponding band is associated with the K' Fermi point of the graphene. In addition, the angular momentum determines the band edge energy Δ_i . In the large- d limit, $\Delta_i = \hbar v_F L_i$, where v_F is the Fermi velocity of graphene. Therefore, in this limit, energy and momentum conservation are simultaneously satisfied for the electrons at the bottom of the third and the fourth bands. However, for finite-diameter tubes, $\Delta_3 < \Delta_2 + 2\Delta_1$ in $\text{mod}(n-m,3)=1$ chirality and $\Delta_4 < \Delta_1 + 2\Delta_2$ in $\text{mod}(n-m,3)=-1$ chirality. This pushes the lowest impact ionization threshold energy E_{th3} of a (25, 0) CNT in the third band to energies higher than the band edge Δ_3 , i.e., $E_{th3} > \Delta_3$, and a power law dependence is obtained, $\Gamma_{ii3} \propto (E - E_{th3})^{\alpha}$ with $\alpha \approx 2$. At the bottom of the fourth band Δ_4 , energy and momentum conservation laws are simultaneously satisfied such that the threshold energy E_{th4} coincides with the bottom of the band Δ_4 , i.e., $E_{th4} = \Delta_4$. The energy dependence of the scattering rate at the onset in the fourth band is similar to that of a step function $\Gamma_{ii4} \propto \Theta(E - E_{th4})$. In a (26,0) tube the impact ionization threshold in the third band coincides with Δ_3 , i.e., $E_{th3} = \Delta_3$, and it is higher than Δ_4 in the fourth band, i.e., $E_{th4} > \Delta_4$. For impact ionization to take place in the first (second) band via the decay channel $e_1^1 = e_1^1 + e_1^1 + h_1^{-1}$ ($e_2'^2 = e_2'^2 + e_1^1 + h_1^{-1}$), the threshold energy must be at least $E_{th1} \geq 3\Delta_1$ ($E_{th2} \geq \Delta_2 + 2\Delta_1$) and momentum conservation along the one-dimensional (1D) wave vector in nonparabolic bands brings the threshold for the first (second) bands to energies beyond the scale of Fig. 1(a).²⁴

In impact excitation, the exciton state formed has an ef-

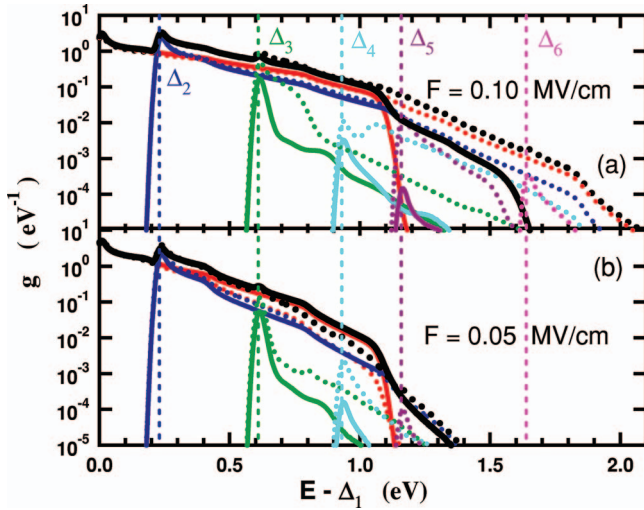


FIG. 2. (Color) Electron distribution function in a (25,0) nanotube at applied electric field of $F=(a)$ 0.1 and (b) 0.05 MV/cm as a function of energy in the first six conduction bands shown in red, blue, green, cyan, magenta, and light red, respectively. Black curves are the total distributions. In (a) solid curves use impact excitation and dotted curves impact ionization scattering rates with phonons at $T=300$ K. In (b) we use impact excitation scattering, solid curves use phonon scattering at $T=300$ K, and dotted curves use acoustic phonon scattering at $T_{ac}=300$ K and optical phonon scattering, at $T_{op}=1500$ K.

fective mass enhanced by 30% over the free particle value (m_e+m_h), due to the Coulomb interaction.²⁵ (We find that the magnitude of the mass enhancement depends on the strength of Coulomb interaction as $1/\epsilon$, independent of tube chirality.) This mass enhancement lowers the threshold energy. Indeed, in the limit of infinite effective mass, the exciton dispersion is flat, and therefore energy and angular momentum conservation alone would determine the impact excitation threshold. Thus, the impact excitation thresholds of the first two conduction bands [Fig. 1(b)] are significantly reduced from the impact ionization values.²⁴ At the onset of impact excitation, the third and the fourth band electrons can decay as $e_3^4=e_2^2+E_{11}^2$ or $e_3^4=e_1^1+E_{12}^3$ and $e_4^5=e_2^2+E_{12}^3$ or $e_4^5=e_1^1+E_{22}^4$. The relative efficiencies of the two decay channels depend on tube chirality and electron energy.

In electro-optical applications, we need to know the effect of impact excitation scattering on the excited state production rate. This depends on the hot carrier distribution function, which we calculate by solving the steady-state multi-band Boltzmann equation in the presence of an electric field, electron-phonon scattering modeled as in Ref. 17, and either impact ionization Eq. (1) or impact excitation scattering Eq. (3). The results are shown in Fig. 2. At energies above the optical phonon energy of about 180 meV, the carrier distribution is determined by the field F and the optical phonon mean free path λ_{op} . The probability that an electron is accelerated to an energy $E=eF\lambda$ over a length λ without being scattered by an optical phonon is $\exp(-\lambda/\lambda_{op})$. Therefore, the carrier distribution g , for energies above the optical phonon and below the impact excitation (ionization) threshold, is expected to follow $g(E) \propto \exp(-E/eF\lambda_{op})$, as seen in Fig. 2.

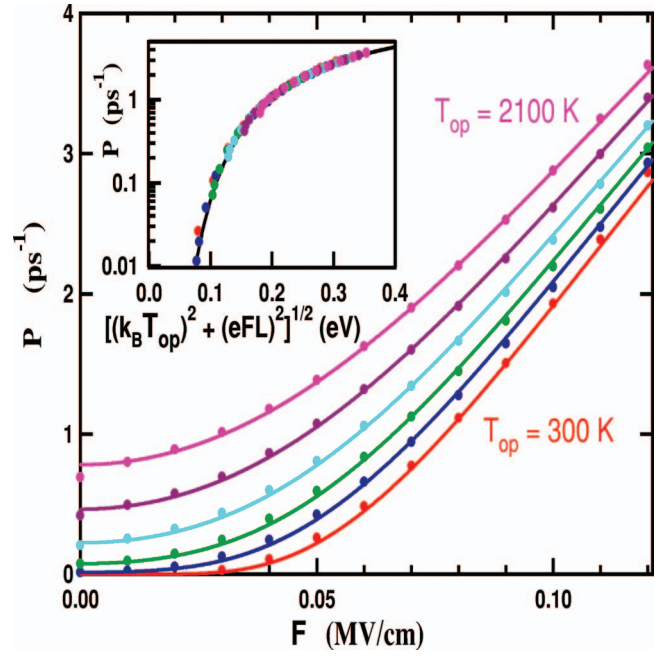


FIG. 3. (Color) Exciton production rate P per unit carrier in a (25,0) tube as function of the electric field for acoustic phonon scattering at $T_{ac}=300$ K and different optical phonon temperatures (from bottom to top) $T_{op}=300$ (red), 900 (blue), 1200 (green), 1500 (cyan), 1800 (magenta), and 2100 K (light red) along with the best fit to Eq. (5) for $\lambda_{op}=25$ nm, $E_t=0.57$ eV, and $P_0=18$ ps⁻¹. The inset shows scaling of all the calculations with the effective temperature in accord with Eq. (5).

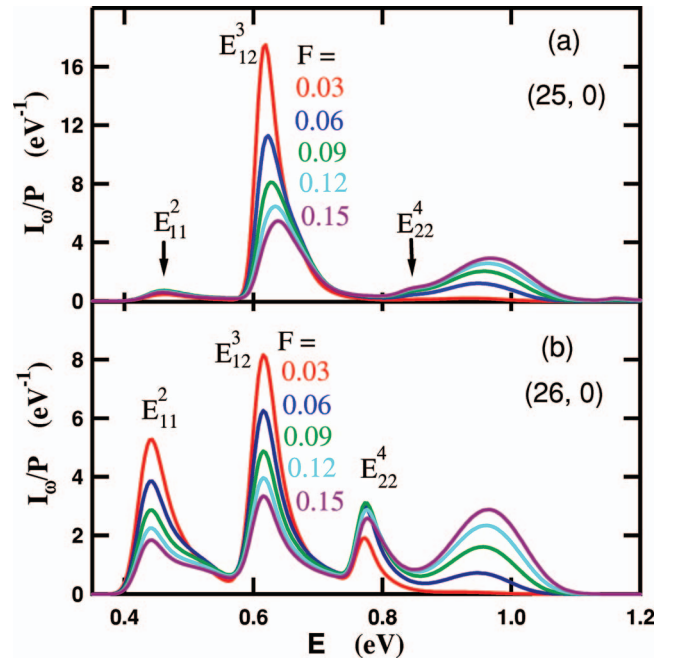


FIG. 4. (Color) Energy distribution I_w of excitons produced in the impact excitation process in (a) a (25,0) tube and (b) a (26,0) tube with phonons at $T=300$ K and different applied electric fields F in MV/cm: 0.03, red; 0.06, blue; 0.09, green; 0.12, cyan; 0.15, magenta; and normalized to the total production rate $P=\int I_w d\omega$.

Above the impact excitation (ionization) threshold, the scattering is an order of magnitude larger and so is the slope $d \ln[g(E)]/dE$, as in Fig. 2. The higher threshold for impact ionization results in a “hotter” carrier distribution than in the case of impact excitation [Fig. 2(a)].

The nonequilibrium phonon effect on the carrier distribution is shown in Fig. 2(b). Although at optical phonon temperature $T_{op}=1500$ K, the phonon scattering rate is a factor 1.7 larger than at room temperature, the slope $d \ln[g(E)]/dE$, for energies below the impact excitation threshold, is similar to the $T_{op}=300$ K case. On the other hand, the hot carrier tail above the impact excitation threshold significantly increases with T_{op} , which in turn increases the exciton production rate.

The exciton production rate itself is given by the product of the carrier distribution, as in Fig. 2, and the impact excitation scattering rate, as in Fig. 1(b), and it is shown in Fig. 3. We find that the rate P can be well fitted by the following equation:

$$P = P_0 \exp\left(-\frac{E_t}{\sqrt{(k_B T_{op})^2 + (eF\lambda_{op})^2}}\right), \quad (5)$$

where E_t is the impact excitation threshold energy and P_0 is a constant. The form of Eq. (5) resembles the Boltzmann distribution with an effective temperature in the presence of a field. The inset of Fig. 3 shows an excellent scaling of the exciton production rate with the effective temperature. The diameter dependence of the fit parameters in Eq. (5) for

$1 < d < 2$ nm is very simple: $E_{th} \approx 1.22$ (eV nm)/ d , $\lambda_{op} \approx 14 \times d$, while $P_0 \approx 18$ ps⁻¹ is nearly diameter independent.

Excitons in nanotubes can be created either by optical pumping as in photoluminescence experiments, or by electrical excitation as in electroluminescence. In the photoluminescence case, the energy of the created excitons follows the photon energy of the excitation light source, and the angular momentum distribution is determined by the dipole selection rules. In the impact excitation process, the energy distribution of the generated excitons depends on the applied bias and it is not subject to the same selection rules. In Fig. 4 we plot the distribution function of the initially created excitons at different fields. The distribution has several distinct peaks, which we identify by analyzing the contributions from excitons with different angular momenta. At the onset of impact excitation, the third- and the fourth-band electrons generate the low-energy excitons with finite angular momenta E_{11}^2 , E_{12}^3 , E_{22}^4 , whereas at higher bias electrons in the first band produce unbound excitons of zero angular momentum, which contribute significantly to a broad continuum at energy about 0.9 eV in Fig. 4.

We conclude that CNTs and other 1D systems are characterized by unusually high impact excitation rates and can be used as efficient exciton sources to be employed in fundamental studies of interacting boson systems at high densities and in opto-electronic device applications.

*Corresponding author. Electronic address: vperebe@us.ibm.com

†Electronic address: avouris@us.ibm.com

¹Ph. Avouris, MRS Bull. **29**, 403 (2004).

²J. A. Misewich, R. Martel, Ph. Avouris, J. C. Tsang, S. Heinze, and J. Tersoff, Science **300**, 783 (2003).

³M. Freitag, V. Perebeinos, J. Chen, A. Stein, J. Tsang, J. Misewich, R. Martel, and Ph. Avouris, Nano Lett. **4**, 1063 (2004).

⁴M. Freitag, J. Chen, J. Tersoff, J. C. Tsang, Q. Fu, J. Liu, and Ph. Avouris, Phys. Rev. Lett. **93**, 076803 (2004).

⁵J. Chen, V. Perebeinos, M. Freitag, J. Tsang, Q. Fu, J. Liu, Ph. Avouris, Science **310**, 1171 (2005).

⁶L. Marty, E. Adam, L. Albert, R. Doyon, D. Ménard, and R. Martel, Phys. Rev. Lett. **96**, 136803 (2006).

⁷T. Ando, J. Phys. Soc. Jpn. **66**, 1066 (1997).

⁸C. D. Spataru, S. Ismail-Beigi, L. X. Benedict, and S. G. Louie, Phys. Rev. Lett. **92**, 077402 (2004).

⁹V. Perebeinos, J. Tersoff, and Ph. Avouris, Phys. Rev. Lett. **92**, 257402 (2004).

¹⁰F. Wang, G. Dukovic, L. E. Brus, and T. F. Heinz, Science **308**, 838 (2005).

¹¹J. Maultzsch, R. Pomraenke, S. Reich, E. Chang, D. Prezzi, A. Ruini, E. Molinari, M. S. Strano, C. Thomsen, and C. Lienau, Phys. Rev. B **72**, 241402(R) (2005).

¹²X. Qiu, M. Freitag, V. Perebeinos, P. Avouris, Nano Lett. **5**, 749 (2005).

¹³We compare rates 0.5 eV above the threshold with those in bulk semiconductors used in Monte Carlo simulations. See, for example, A. Kuligk, N. Fitzer, and R. Redmer, Phys. Rev. B **71**, 085201 (2005).

¹⁴Z. Yao, C. L. Kane, and C. Dekker, Phys. Rev. Lett. **84**, 2941 (2000).

¹⁵A. Javey, J. Guo, M. Paulsson, Q. Wang, D. Mann, M. Lundstrom, and H. Dai, Phys. Rev. Lett. **92**, 106804 (2004).

¹⁶J. Y. Park, S. Rosenblatt, Y. Yaish, V. Sazonova, H. Ustunel, S. Braig, T. A. Arias, P. Brouwer, and P. L. McEuen, Nano Lett. **4**, 517 (2004).

¹⁷V. Perebeinos, J. Tersoff, and Ph. Avouris, Phys. Rev. Lett. **94**, 086802 (2005).

¹⁸M. Lazzeri, S. Piscanec, F. Mauri, A. C. Ferrari, and J. Robertson, Phys. Rev. Lett. **95**, 236802 (2005).

¹⁹E. Pop, D. Mann, J. Cao, Q. Wang, K. Goodson, and H. Dai, Phys. Rev. Lett. **95**, 155505 (2005).

²⁰P. T. Landsberg, *Recombination in Semiconductors* (Cambridge University Press, Cambridge, U.K., 1991).

²¹E. K. Chang and E. L. Shirley, Phys. Rev. B **66**, 035106 (2002).

²²Due to the mutual cancellation of the exciton binding and the free particle GW corrections (Ref. 8), we use the scissor approximation for the free particle spectra with a scissor value equal to the binding energy of the first optically active exciton.

²³G. Dukovic, F. Wang, D. Song, M. Y. Sfeir, T. F. Heinz, and L. E. Brus, Nano Lett. **5**, 2314 (2005).

²⁴For two parabolic valence and conduction bands the onset of the impact excitation has the usual power law dependence (Ref. 20) $\Gamma \propto (E - E_{th})^\alpha$ with $\alpha=2$ and $E_{th} \approx 1.5E_g$, where E_g is the band gap. Due to the nonparabolicity of the CNT bands, in a (25,0) tube $E_{th1} = \Delta_1 + 2.6$ eV, $E_{th2} = \Delta_1 + 4.6$ eV, or $E_{th} \approx 6.5E_g$.

²⁵V. Perebeinos, J. Tersoff, and Ph. Avouris, Nano Lett. **5**, 2495 (2005).